© 2015. Published by The Company of Biologists Ltd | The Journal of Experimental Biology (2015) 218, 2039-2048 doi:10.1242/jeb.118182

RESEARCH ARTICLE

Internal carbonic anhydrase activity in the tissue of scleractinian corals is sufficient to support proposed roles in photosynthesis and calcification

Brian M. Hopkinson[1,*], Anna L. Tansik[1] and William K. Fitt[2]

ABSTRACT

Reef-building corals import inorganic carbon (C_i) to build their calcium carbonate skeletons and to support photosynthesis by the symbiotic algae that reside in their tissue. The internal pathways that deliver C_i for both photosynthesis and calcification are known to involve the enzyme carbonic anhydrase (CA), which interconverts CO_2 and HCO_3^-. We have developed a method for absolute quantification of internal CA (iCA) activity in coral tissue based on the rate of ^{18}O-removal from labeled C_i. The method was applied to three Caribbean corals (*Orbicella faveolata*, *Porites astreoides* and *Siderastrea radians*) and showed that these species have similar iCA activities per unit surface area, but that *S. radians* has ~10-fold higher iCA activity per unit tissue volume. A model of coral C_i processing shows that the measured iCA activity is sufficient to support the proposed roles for iCA in C_i transport for photosynthesis and calcification. This is the case even when iCA activity is homogeneously distributed throughout the coral, but the model indicates that it would be advantageous to concentrate iCA in the spaces where calcification (the calcifying fluid) and photosynthesis (the oral endoderm) take place. We argue that because the rates of photosynthesis and calcification per unit surface area are similar among the corals studied here, the areal iCA activity used to deliver C_i for these reactions should also be similar. The elevated iCA activity per unit volume of *S. radians* compared with that of the other species is probably due to the thinner effective tissue thickness in this species.

KEY WORDS: Inorganic carbon, Cnidarians, *Symbiodinium*, Modelling

INTRODUCTION

Active inorganic carbon (C_i) supply pathways are required to support the high rates of photosynthesis and calcification that have allowed reef-building corals to thrive and create the extensive reef structures that support coral reef ecosystems. These pathways must deliver C_i to the symbiotic dinoflagellates (of the genus *Symbiodinium*) that reside primarily within the upper endodermal layer of the coral (Furla et al., 2000b; Bertucci et al., 2013). The algae further concentrate C_i obtained from the coral using a CO_2 concentrating mechanism and ultimately convert the C_i to CO_2 for fixation in the Calvin cycle (Leggat et al., 1999). At the same time, C_i is routed to the calcifying space at the interface between the existing $CaCO_3$ skeleton and the ectodermal cells of the coral animal where the C_i is converted to CO_3^{2-} and combined with Ca^{2+} to form new skeleton (Tambutte et al., 2011). Much of the carbon fixed by the symbiotic algae is transported to and then respired by the coral. The coral recycles most of the respired CO_2, using it for both photosynthesis and calcification (Furla et al., 2000b). The full details of these C_i supply and recovery pathways are not fully understood, but it is clear that they are complicated and interconnected (Fig. 1; Tambutte et al., 2011; Bertucci et al., 2013).

A critical component of nearly all C_i supply pathways is the enzyme carbonic anhydrase (CA). This enzyme catalyzes the hydration of CO_2 and dehydration of HCO_3^- moving the CO_2/HCO_3^- system towards chemical equilibrium. CAs play diverse roles in organisms and are involved in CO_2 uptake, gas exchange, pH homeostasis and internal C_i transport pathways (Henry, 1996; Badger, 2003; Boron, 2004). In corals and related cnidarians, CAs are involved in supplying C_i for both photosynthesis and calcification. A surface-associated extracellular CA is involved in CO_2 uptake (Furla et al., 2000a; Tansik et al., in press), and internal CAs are likely used to convert newly imported CO_2 to HCO_3^-, and for recovery of respired CO_2 as HCO_3^- (Fig. 1; Bertucci et al., 2013). These transformations serve to concentrate C_i as HCO_3^-, which is the form of C_i typically concentrated by organisms because as a charged molecule it does not pass easily through membranes. In contrast, biological membranes are highly permeable to CO_2, a small, uncharged molecule (Gutknecht et al., 1977). Accumulated HCO_3^- can then be transported to the symbiotic algae, possibly via SLC4-type bicarbonate transporters, which have recently been identified in the genomes and transcriptomes of several coral species (Moya et al., 2012; Kenkel et al., 2013), or converted to CO_2 in the oral endoderm for uptake by *Symbiodinium* (Al-Moghrabi et al., 1996; Bertucci et al., 2010). Inhibition of CAs reduces the photosynthetic rates of corals, showing that this enzyme is essential for maintaining high rates of photosynthesis (Weis et al., 1989; Al-Moghrabi et al., 1996).

CAs are also involved in calcification (Goreau, 1959), probably as part of the C_i transport system in coral tissue and within the calcifying fluid to enhance calcification. C_i used for calcification is a mix of respired CO_2, HCO_3^- transported through coral tissue, and C_i obtained from direct seawater import to the calcifying fluid (Furla et al., 2000b; Cohen and McConnaughey, 2003; Gagnon et al., 2012). The C_i transport pathways for calcification are thus broadly similar to those used to transport C_i for photosynthesis, and so the likely roles of CA in these transport steps are analogous. In several corals (*Stylophora pistillata*, *Acropora hebes* and *Tubastrea aurea*), CA has been localized directly to the calicoblastic ectoderm, the cell layer that mediates calcification and is in direct contact with the calcifying fluid, or the skeletal matrix and it has been suggested that CA may be secreted into the calcifying fluid (Isa and Yamazato, 1984; Tambutte et al., 2007; Moya et al., 2008). CA in the calcifying fluid would convert respired CO_2 to HCO_3^- for subsequent conversion to CO_3^{2-} (Fig. 1; Cohen and McConnaughey, 2003).

[1]Department of Marine Sciences, University of Georgia, Athens, GA 30602, USA. [2]School of Ecology, University of Georgia, Athens, GA 30602, USA.

*Author for correspondence (bmhopkin@uga.edu)

Received 10 December 2014; Accepted 20 April 2015

The Journal of Experimental Biology (2015) 218, 2039-2048 doi:10.1242/jeb.118182

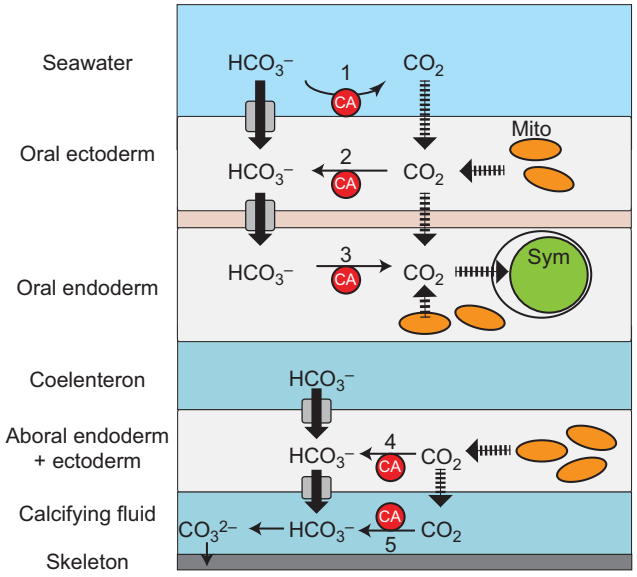

Fig. 1. Inorganic carbon (C_i) fluxes and potential roles of carbonic anhydrase (CA) in coral C_i processing. The figure is based primarily on Bertucci et al. (2013). (1) External carbonic anhydrase (eCA) on the oral surface converts HCO_3^- to CO_2, which then passively diffuses in the oral ectoderm as the result of a concentration gradient. (2) CA in the oral ectoderm may convert imported and respired CO_2 to HCO_3^-, which is then transported into the oral endoderm. Respiration occurs in the mitochondria (Mito, orange ovals). (3) In the oral endoderm, HCO_3^- can be converted to CO_2 by CA for uptake by *Symbiodinium* (Sym, green circle). (4) Respired CO_2 can be converted to HCO_3^- using CA for use in calcification or photosynthesis. (5) CA in the calcifying fluid converts respired CO_2 to HCO_3^- for subsequent use in calcification.

CAs are clearly important in corals and there has been substantial progress in identifying, localizing and in some case characterizing individual CAs. Weis et al. (1989) found that corals contain substantial amounts of CA activity and that zooxanthellate species had significantly more CA than species lacking symbiotic algae. While this work showed that corals have high levels of CA activity, the approach used was not quantitative in an absolute sense, that would, for example, allow the measured rates to be incorporated into models of photosynthesis and calcification (e.g. Hohn and Merico, 2012; Nakamura et al., 2013). Here, we adapted a method that relies on the rate of ^{18}O-removal from labeled C_i to obtain quantitative measurements of internal CA (iCA) activity in corals – in this case *Orbicella faveolata* (Ellis and Solander 1786), *Porites astreoides* Lamarck 1816 and *Siderastrea radians* (Pallas 1766). As the ^{18}O-removal measurement is made on coral homogenate, the method provides a measure of the average iCA activity throughout the corals tissue layers including the calcifying fluid. It is highly unlikely that CA is in fact distributed homogeneously throughout the tissue, and the need for CA localization is explored using a spatially resolved model of C_i processing.

RESULTS

Coral iCA activity

Coral iCA activity was determined by quantitative analysis of ^{18}O-removal catalyzed by purified coral tissue homogenate using a model that includes coral iCA and external (e)CA activity, and *Symbiodinium* iCA activity (see Materials and methods). The method relies on the fact that all CA isoforms accelerate the hydration of CO_2 and dehydration of HCO_3^-, which in turn accelerates the exchange of the ^{18}O label in C_i for ^{16}O from water (Silverman, 1982). In this analysis, CA activity in the purified tissue homogenate is partitioned into various experimentally separable fractions. eCA activity is first measured on intact coral fragments (Tansik et al., in press), and then the coral tissue is removed and homogenized (Fig. 2A). *Symbiodinium* cells are removed from the homogenate by centrifugation and their CA activity is measured. Finally, the purified tissue homogenate is assayed for CA activity, and the iCA activity of the coral is determined by subtracting the contributions of coral eCA and residual *Symbiodinium* iCA from the total CA activity in the purified homogenate.

Determination of coral iCA activity using this approach first requires measurement of coral eCA activity and the algal iCA activity and mass transfer coefficients. The coral eCA activity was measured by an ^{18}O-removal assay on intact coral fragments. These data are presented elsewhere (Tansik et al., in press) and the eCA activities are listed in Table 1. eCA activity varied substantially between taxa with *O. faveolata* having the highest eCA activity, approximately one order of magnitude greater than that of *S. radians* and *P. astreoides*. Algal iCA activity and mass transfer coefficients were measured using an ^{18}O-removal assay on cells freshly isolated from coral tissue. Algal iCA activity also differed among taxa, although activities in all taxa were very high compared with those in other microalgae (Tu et al., 1986; Hopkinson et al., 2013). *Symbiodinium* from *S. radians* had the highest iCA activity, followed by those from *P. astreoides*, and then *Symbiodinium* from *O. faveolata*. CO_2 and HCO_3^- mass transfer coefficients were similar among the taxa, and showed that the cell membranes are highly permeable to CO_2 but impermeable to HCO_3^- like other microalgae (Table 1).

After obtaining coral eCA and algal parameters, coral iCA activity was determined from analysis of the effect of purified coral tissue homogenate on ^{18}O-removal rates. The coral homogenate substantially accelerated the rate of ^{18}O-removal (Fig. 2, Table 2). Addition of the CA inhibitor acetazolamide (AZ) slowed ^{18}O-removal rates to background rates (or even slightly below background rates), verifying that CA activity was responsible for the acceleration (Table 2). Although the potency of AZ differs with CA isoform, the 100 µmol l^{-1} AZ added should be sufficient to fully inhibit most CA isoforms as typical inhibitory constants are <50 nmol l^{-1} (Moya et al., 2008). The fact that ^{18}O-removal rates returned to background levels after addition of AZ confirms that CA activity was effectively inhibited for these corals. Analysis of these data using the ^{18}O-removal model presented in Eqns 3–6 (see Materials and methods) shows that the model fits the data well for all taxa, allowing accurate determination of coral iCA activity. The coral iCA activity can either be normalized by the coral tissue volume to obtain a first-order rate constant, or normalized by coral surface area. The advantage of the first-order rate constant is that it is directly relevant to internal C_i fluxes, can be applied to models of C_i processing in corals and is intuitive. However, normalization by volume treats the iCA as being homogeneously distributed throughout the internal volume of the coral, which is not likely to be the case. When normalized to coral tissue volume, *S. radians* has approximately 10-fold higher iCA activity than both *O. faveolata* and *P. astreoides* (*t*-test, $P<0.05$), but the iCA activities of *O. faveolata* and *P. astreoides* are not significantly different from one another (Fig. 3).

In contrast, when normalized to coral surface area, *O. faveolata* and *S. radians* have similar iCA activity, while *P. astreoides* has approximately half the iCA activity of the other two species. However, only the difference between *S. radians* and *P. astreoides* is statistically significant (*t*-test, $P<0.05$). The overall range in coral

The Journal of Experimental Biology (2015) 218, 2039-2048 doi:10.1242/jeb.118182

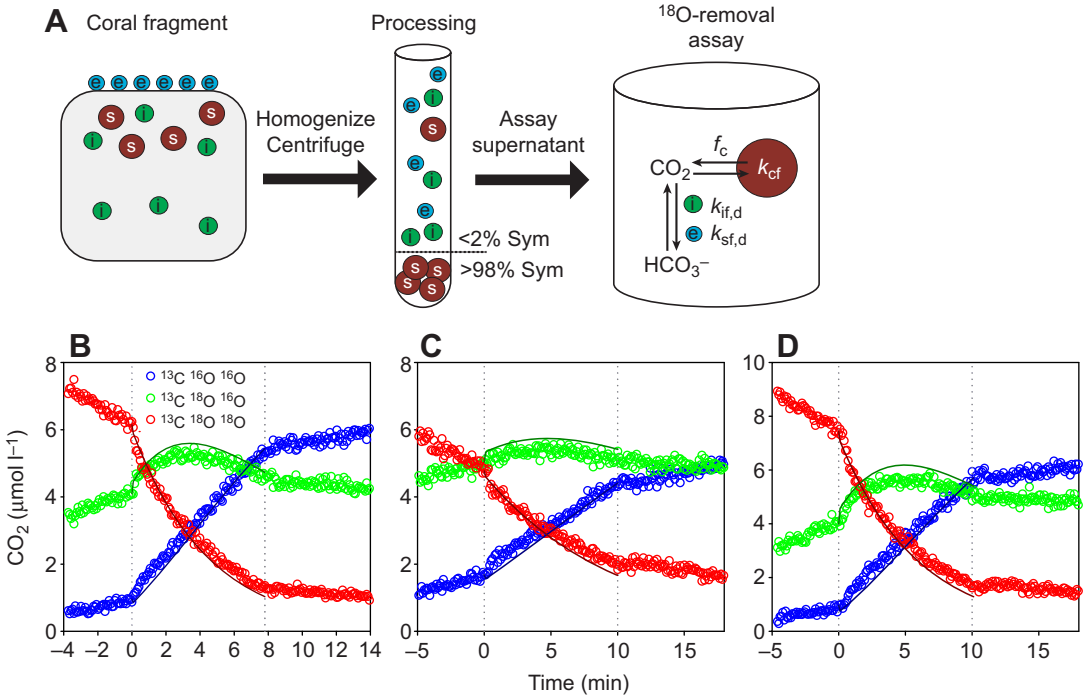

Fig. 2. iCA measurement procedure and sample results. (A) Diagram illustrating iCA measurement procedure. The intact coral fragment contains eCA (e) on the outer surface, iCA (i) within the tissue, and CA within *Symbiodinium* (s, Sym). The tissue is homogenized and then centrifuged to remove *Symbiodinium*. The purified tissue homogenate is then assayed for CA activity using an ^{18}O-removal assay. Key model terms affecting ^{18}O-removal are indicated: $k_{if,d}$, the diluted coral iCA CO_2 hydration rate constant; $k_{sf,d}$, the diluted coral eCA CO_2 hydration rate constant; f_c, the *Symbiodinium* CO_2 mass transfer coefficient; k_{cf}, the *Symbiodinium* CO_2 hydration rate constant (see also Table 1). (B–D) Examples of ^{18}O-CO_2 data for each coral taxa (B: *Orbicella faveolata*, C: *Porites astreoides*, D: *Siderastrea radians*) showing background rates of ^{18}O-removal prior to time zero, acceleration of ^{18}O-removal upon addition of coral tissue homogenate at time zero (first dotted vertical line) and a slow down in the ^{18}O-removal rate after addition of a CA inhibitor (acetazolamide, AZ) at 7–10 min (second dotted vertical line). The solid lines are fits to the data of the ^{18}O-removal model used to determine coral iCA activity. The key in B indicates which symbols represent different CO_2 isotopic species: $^{13}C^{16}O^{16}O$ (blue circles), $^{13}C^{18}O^{16}O$ (green circles), and $^{13}C^{18}O^{18}O$ (red circles).

iCA activity between taxa is lower when normalized to surface area (2.8×) than when normalized by volume (9×), and it is notable that photosynthetic rates per unit area are very similar among the coral species (Fig. 3).

Contribution of coral eCA and algal iCA to ^{18}O-removal

Obtaining the coral iCA activity requires accounting for the effects of coral eCA and algal iCA on ^{18}O-removal catalyzed by the purified tissue homogenate (see Materials and methods; supplementary material Fig. S1). The greater the contribution of these additional components to ^{18}O-removal, the more difficult it is to accurately determine coral iCA activity. We assessed the effects of these additional components in two ways: first, graphically, showing how the ^{18}O-removal model predicts that ^{18}O-CO_2 isotopologues would evolve as components are added, and second, by determining how neglecting the additional components in the model would affect inferred coral iCA activity.

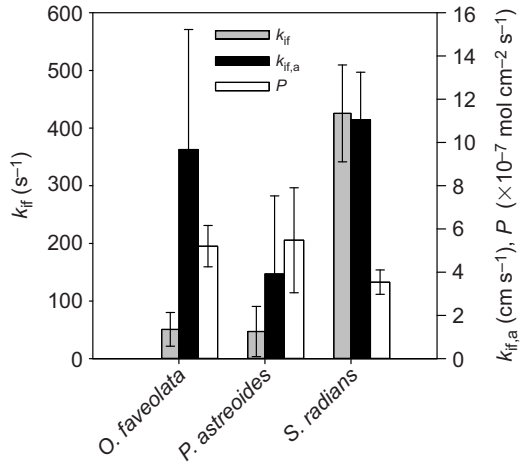

Fig. 3. Coral iCA activity normalized to coral tissue volume (k_{if}) and to coral surface area ($k_{if,a}$) and net photosynthetic rates (P) for each coral taxon. Error bars represent s.d.

We ran the ^{18}O-removal model in a forward (predictive) sense first, considering how the ^{18}O-CO_2 isotopologues would evolve in the absence of any CA activity, and then sequentially adding the effects of algal iCA, coral eCA and coral iCA. Fig. 4 shows representative results for each taxon, but similar results were obtained for each sample within a taxon. The effect of residual *Symbiodinium* on ^{18}O-removal was quite small in all taxa. Centrifugation removes more than 98% of the *Symbiodinium* cells from the crude homogenate, which is sufficient to effectively eliminate any interference for determination of coral iCA activity. In general, the effects of coral eCA were also small, though in *O. faveolata*, which had the highest eCA activity, coral eCA could have a substantial effect on ^{18}O-removal. This analysis indicates that accounting for the effect of coral eCA activity is important, but that residual *Symbiodinium* contribute little to ^{18}O-removal as long as the centrifugation is effective.

To make a more quantitative assessment, we examined the effects of neglecting coral eCA and algal iCA on the inferred coral iCA activity. When these components are neglected in the model, their

The Journal of Experimental Biology (2015) 218, 2039-2048 doi:10.1242/jeb.118182

Table 1. Description of parameters used in the model and values for each coral species

Symbol	Definition	*Orbicella faveolata*	*Porites astreoides*	*Siderastrea radians*	Units
$\mathbf{c}_e$, $\mathbf{c}_i$	CO_2 concentration of the bulk solution and inside *Symbiodinium* cells				mol cm^{-3}
$\mathbf{b}_e$, $\mathbf{b}_i$	HCO_3^- concentration of the bulk solution and inside *Symbiodinium* cells				mol cm^{-3}
G, **H***	Stoichiometric matrices for interconversion of ^{18}O-CO_2 and ^{18}O-HCO_3^- species				–
k_{uf}, k_{ur}	Background CO_2 hydration, HCO_3^- dehydration rate constants	0.14	0.16	0.14	s^{-1}
k_{sf}, k_{sr}	Coral eCA-catalyzed CO_2 hydration, HCO_3^- dehydration rate constants	6.3±0.3	0.45±0.29	0.26±0.44	cm s^{-1}
k_{if}, k_{ir}	Coral iCA-catalyzed CO_2 hydration, HCO_3^- dehydration rate constants				s^{-1}
k_{cf}, k_{cr}	*Symbiodinium* iCA-catalyzed CO_2 hydration, HCO_3^- dehydration rate constants	970±350	1450±370	2120±230	s^{-1}
f_c	*Symbiodinium* CO_2 mass transfer coefficient	$1.6(\pm0.1)\times10^{-7}$	$1.7(\pm0.3)\times10^{-7}$	$1.5(\pm0.1)\times10^{-7}$	cm^3 s^{-1}
f_b	*Symbiodinium* HCO_3^- mass transfer coefficient	$1.1(\pm0.7)\times10^{-11}$	$1.4(\pm0.4)\times10^{-12}$	$6.7(\pm9.0)\times10^{-12}$	cm^3 s^{-1}
N	Concentration of *Symbiodinium*				cells cm^{-3}
V_{cell}	Volume of *Symbiodinium* cell	2.7×10^{-10}	2.7×10^{-10}	2.7×10^{-10}	cm^3
V_{add}	Volume of homogenate added to assay	0.1–0.2	0.1–0.2	0.1–0.2	cm^3
V_{hom}	Total volume of homogenate	24–38	40	27–37	cm^3
V_e	Assay volume	1	1	1	cm^3
A_c	Coral surface area removed	7.7–11.2	8.1–11.3	6.0–8.4	cm^2
L_c	Average coral tissue thickness	1.9	2.3	1.3	mm
ϕ	Porosity	1	0.36	0.20	
ϕL_c	Effective tissue thickness (tissue volume per unit surface area)	1.9	0.83	0.26	mm

eCA, external carbonic anhydrase; iCA, internal carbonic anhydrase.
*See Hopkinson et al. (2011).

contribution to ^{18}O-removal will be attributed to coral iCA activity, the unknown model parameter, increasing the inferred coral iCA activity. As shown in Fig. 5, neglecting algal iCA resulted in only minor increases in the inferred coral iCA activity (<7%), consistent with the graphical analysis showing that residual algal cells have negligible effects on ^{18}O-removal. For *P. astreoides* and *S. radians*, neglecting coral eCA activity led to at most moderate increases in inferred coral iCA activity (<15%), but for *O. faveolata* the effects were much more significant, especially for one specimen that had low iCA activity.

C_i processing model analysis

A one-dimensional model of coral C_i processing that includes active HCO_3^- transport, passive CO_2 transport, CA-catalyzed interconversion of CO_2 and HCO_3^-, photosynthesis and calcification was used to help interpret the measured iCA activities. C_i processing pathways in corals are still under study and are in some cases controversial. For example, electron microscopy of the tissue–skeleton interface suggests that there is little to no calcifying fluid (Clode and Marshall, 2002), but more sizable reservoirs of calcifying fluid have been detected as high pH regions in confocal microscopic imaging (Venn et al., 2011). The C_i pathways in the model were chosen from among proposed routes in a way that maximizes iCA requirements (using iCA in all the reactions shown in Fig. 1). The model is schematic and is used here only to assess the suitability of measured iCA activity to perform proposed functions and to explore iCA requirements. It is not a general mechanistic model of coral C_i processing. Most notably, the metabolic fluxes (photosynthesis, respiration, calcification, HCO_3^- transport) are specified based on measured rates or to achieve mass balance, rather than being determined mechanistically using enzyme kinetics.

Table 2. ^{18}O-removal rates calculated as the slope of a linear fit through natural log-transformed ^{18}O atom fraction data

	^{18}O-removal ($\times10^{-4}$ s^{-1})		
Coral	Background	Homogenate	Homogenate+AZ
O. faveolata	3.5±0.3	3.9–14.2	2.5±0.2
P. astreoides	2.6±0.3	3.5–6.5	2.1±0.1
S. radians	2.8±0.4	5.0–12.5	1.7±0.1

Background rates are means±s.d. obtained prior to the addition of coral homogenate. Rates after the addition of coral homogenate are reported as the range among samples, as these rates are not expected to be constant because of variation in CA activity and volume of homogenate added. Acetazolamide (AZ) was then added to selected samples and the means±s.d. are reported for this phase.

First, the model was run with an iCA activity of 50 s^{-1}, approximately what was measured in *O. faveolata* and *P. astreoides*, distributed homogeneously throughout the coral tissue layers and calcifying fluid (Fig. 6). This iCA activity was able to support rates of photosynthesis, calcification and respiration measured in *O. faveolata*, but in the case of calcification the iCA activity was only just sufficient. In the oral ectoderm, iCA catalyzes the conversion of newly imported and respired CO_2 to HCO_3^-. Although CO_2 concentrations in this layer are lower than in seawater, driving the CO_2 influx, they are in fact above equilibrium concentrations with HCO_3^- because HCO_3^- concentrations are low as a result of active export to the underlying oral endoderm. The active transport of HCO_3^- across membranes would be mediated by transporters such as the SLC4-type HCO_3^- transporters recently identified in corals (Moya et al., 2012; Kenkel et al., 2013). In the oral endoderm, HCO_3^- is imported and converted to CO_2 by iCA. The CO_2 is then consumed by the *Symbiodinium* that reside in the oral endoderm layer, lowering CO_2 concentrations below equilibrium values. CO_2 and HCO_3^- are in equilibrium in the coelenteron where no metabolic processes occur. In the aboral tissue layer, respiration produces CO_2, part of which is converted to

The Journal of Experimental Biology (2015) 218, 2039-2048 doi:10.1242/jeb.118182

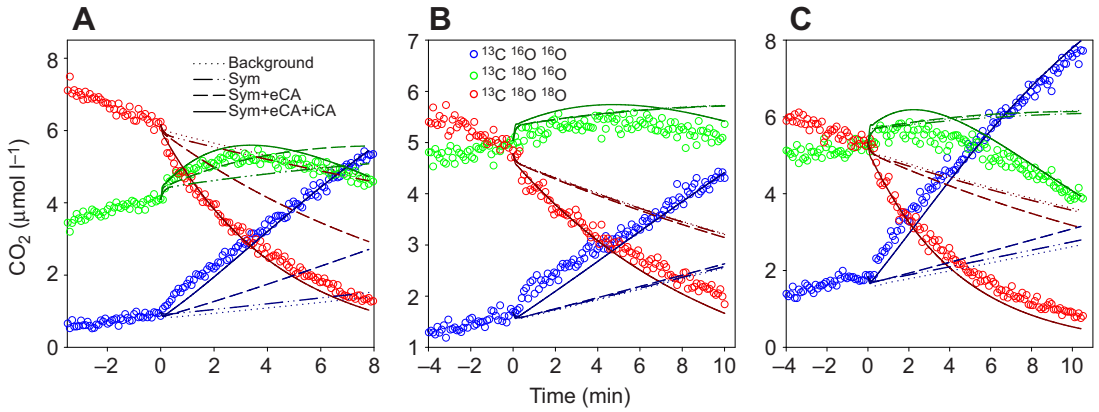

Fig. 4. Contribution of CA components in the coral homogenate to total ^{18}O-removal. The ^{18}O-removal model was run in a predictive sense, sequentially adding components to the model (Sym, *Symbiodinium* iCA; eCA, coral eCA; iCA, coral iCA). A: *O. faveolata*, B: *P. astreoides*, C: *S. radians*.

HCO_3^- by CA and the remainder of which diffuses into the calcifying fluid where it is then converted to HCO_3^- by CA for use in calcification.

The iCA activity in the calcifying fluid was only just sufficient to support the measured rates of calcification for *O. faveolata*. This can be most clearly seen from the low HCO_3^- concentration in the calcifying fluid, indicating high rates of removal relative to input, and in the nearly 100% deviation of CO_2 concentrations from equilibrium with HCO_3^- (Fig. 6C). Greater deviations from equilibrium (either positive or negative) indicate that maximal CO_2 hydration or HCO_3^- dehydration fluxes are being reached because the maximal net fluxes occur when the product concentration (HCO_3^- for hydration, CO_2 for dehydration) is zero. Consequently, the deviation of CO_2 from equilibrium with HCO_3^- is used as an index of the effectiveness of the C_i processing system, with moderate deviation (<25%) being acceptable, but further deviation indicating the system is near its maximal capacity. We note that in our simplistic model, meant only to explore the role of iCA, there is no dependence of the calcification rate on HCO_3^- or CO_3^{2-} concentrations. The low HCO_3^- and CO_3^{2-} concentrations in this model would probably not provide a high enough aragonite saturation state to obtain the observed calcification rates (e.g. Burton and Walter, 1987).

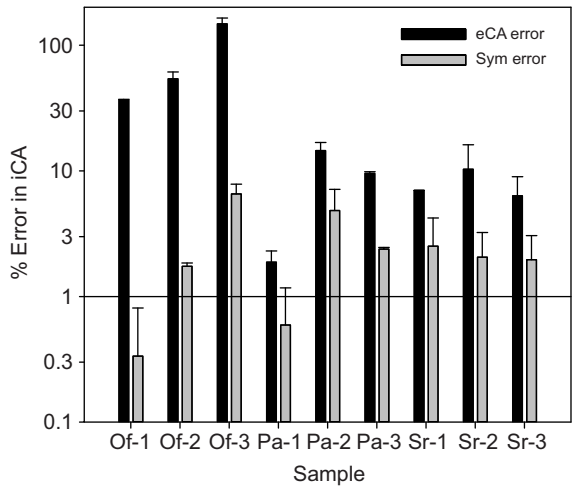

Fig. 5. Effect of neglecting contributions of *Symbiodinium* iCA and coral eCA on the determination of coral iCA activity. Data for three samples each of *O. faveolata* (Of), *P. astreoides* (Pa) and *S. radians* (Sr) are shown.

Running the model with higher (500 s^{-1}) and lower (5 s^{-1}) iCA activities shows that the observed iCA activity is nearly optimal for supporting the required C_i fluxes and keeping CO_2 and HCO_3^- concentrations close to equilibrium (Fig. 6). Decreasing iCA 10-fold leads to significant deviations of CO_2 from equilibrium with HCO_3^- and the model is only able to support calcification at 40% of the observed rate. This results in a lower HCO_3^- concentration in the calcifying fluid compared with that in models with higher iCA activity. Increasing iCA 10-fold does lead to nearly complete equilibrium between CO_2 and HCO_3^- throughout the coral, but there are no performance gains directly associated with this increase.

The C_i processing model was used to explore the effect of changes in photosynthetic rate and tissue thickness on required iCA activity. The model with a homogeneous iCA activity similar to that measured in the reef corals (50 s^{-1}) and metabolic rates of *O. faveolata* was used as a reference point. First, the net photosynthetic rate was varied (with the respiration rate being set equal to the net photosynthetic rate) and the iCA activity was optimized to obtain the same average CO_2 deviations in each tissue layer as in the base model. The average CO_2 deviations are used here as a measure of the effectiveness of CA at supplying C_i for transport or metabolism. The required iCA activity scaled approximately linearly with the photosynthetic rate (Fig. 7A). Next, the tissue thickness was varied from the reference point (2 mm), keeping the metabolic rates per unit surface area constant, and the iCA activity was optimized to match CO_2 deviations to the base model. The required iCA activity per unit volume increased rapidly as the tissue thickness decreased and conversely decreased as the tissue thickness increased (Fig. 7B). However, the iCA activity per unit surface area was nearly constant, increasing slightly with increasing tissue thickness.

DISCUSSION

CA is a widely distributed enzyme having many isoforms and diverse roles in organisms. It has long been recognized to be important in marine organisms, some of the earliest work being in mollusks (Freeman and Wilbur, 1948; Wilbur and Jodrey, 1955), and more recently its roles in corals and other cnidarians have been investigated (Bertucci et al., 2013). We have developed a method to determine the iCA activity of corals by measuring the acceleration of ^{18}O-removal from labeled C_i catalyzed by purified coral tissue homogenate (Fig. 2, Table 2). iCA activity was measured in three species of

The Journal of Experimental Biology (2015) 218, 2039-2048 doi:10.1242/jeb.118182

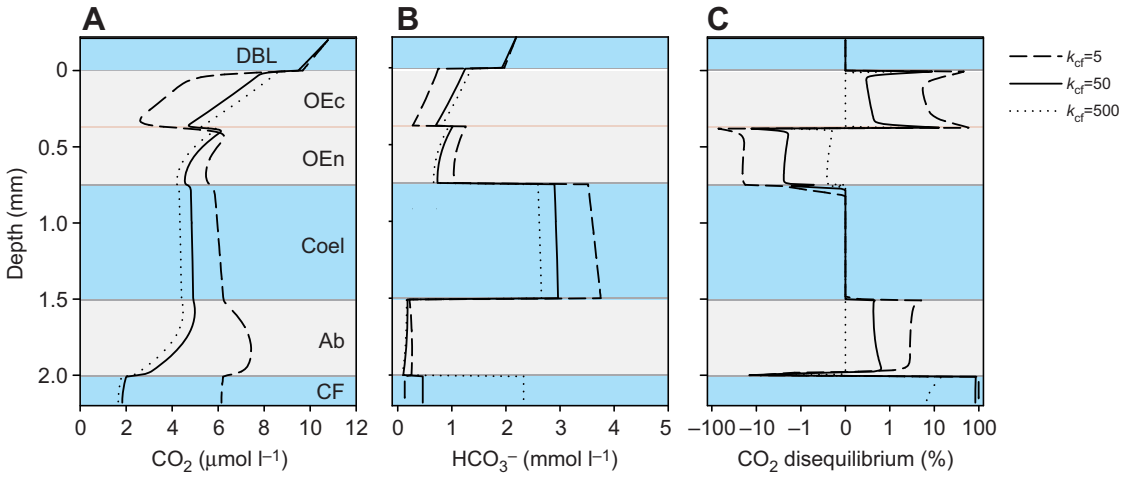

Fig. 6. Results of the spatially resolved C_i processing model. iCA activity was homogeneously distributed throughout the tissue at the rates indicated (k_{cf}). Photosynthetic and calcification rates were the same in the models with measured (50 s^{-1}) and elevated (500 s^{-1}) iCA activity but the calcification rate was reduced to 40% of the original rate in the model with lowered (5 s^{-1}) iCA activity. Plots show (A) the CO_2 concentration, (B) the HCO_3^- concentration and (C) CO_2 deviations from equilibrium with HCO_3^- as a function of depth in the coral tissue. Background colors and abbreviations in A indicate the model layers: DBL, diffusive boundary layer; OEc, oral ectoderm; OEn, oral endoderm; Coel, coelenteron; Ab, aboral tissue; CF, calcifying fluid. The thickness of the calcifying fluid has been exaggerated (60×) in the plot for clarity.

Caribbean corals. We found that the two species that inhabit offshore reefs (*O. faveolata*, *P. astreoides*) had similar iCA activity when normalized to tissue volume, whereas a species from Florida Bay (*S. radians*) had ∼10-fold higher iCA activity (Fig. 3). In contrast, when normalized to coral surface area, *O. faveolata* and *S. radians* had similar iCA activities, while the iCA activity of *P. astreoides* was lower. Determination of coral iCA activity required removing contributions from residual *Symbiodinum* cells and coral eCA from the total CA activity of the purified coral tissue homogenate. Residual *Symbiodinium* cell numbers were always low and did not significantly affect determination of coral iCA activity (Figs 4, 5). In *P. astreoides* and *S. radians*, eCA activity was also not a major issue, but in *O. faveolata*, which had very high eCA activity, accounting for eCA activity was essential for accurate determination of coral iCA activity.

The coral iCA activity measurement includes all CAs in the cytoplasm, on internal membranes, in the coelenteron and in the calcifying fluid. Membrane-bound CAs have been localized near the symbiosome membrane presumably to facilitate C_i delivery to *Symbiodinium* (Weis, 1993; Al-Moghrabi et al., 1996), and could also be facing the coelentron, or attached to the calicoblastic cells to aid calcification (Moya et al., 2008). iCAs have also been identified within the cytoplasm of the oral and aboral tissue (Grasso et al., 2008; Bertucci et al., 2011), and within calicoblastic cells (Moya et al., 2008), but there are many more CAs in coral genomes that have yet to be localized.

As the iCA measurements required homogenizing the tissue, the measured iCA activity may not precisely match *in vivo* activity. This is always a concern with enzyme assays, but is somewhat less of an issue for CA because it does not require an energy source, though its activity can be regulated by cellular conditions such as redox status (Kikutani et al., 2012). The *in vivo* iCA activity provides complementary rate information to molecular work on coral CAs that has provided more detailed information about CA localization and hence the potential role of individual CA isoforms. While molecular approaches can provide quantitative information about CA activity, this is quite time consuming and difficult, requiring over-expression of active CA proteins followed by assessment of CA activity, and is only rarely done (Moya et al., 2008; Bertucci et al., 2011).

Measured iCA activity is sufficient to fulfill hypothesized roles

A key feature of these measurements is that they are quantitative, allowing calculation of CO_2 hydration or HCO_3^- dehydration rates within coral tissue. Consequently, these iCA activities are suitable for incorporation into models of C_i processing, or for simpler estimates of CO_2 supply for photosynthesis or HCO_3^- production for calcification. Coral CAs have been proposed to play multiple roles in C_i processing (Fig. 1) and an important question is whether the measured iCA activities are sufficient to support these proposed roles. The gross HCO_3^- generation rate (F_b) in the coral can be estimated from the measured iCA activity and the CO_2 concentration in coral tissue as:

$$F_b = k_{if,a}[CO_2], \quad (1)$$

where $k_{if,a}$ is iCA activity normalized to coral surface area, and the gross CO_2 generation rate (F_c) can be calculated from the iCA activity, the CO_2/HCO_3^- equilibrium constant (K_1), the internal pH and the HCO_3^- concentration in coral tissue as:

$$F_c = k_{if,a}\frac{[H^+]}{K_1}[HCO_3^-]. \quad (2)$$

The net CO_2 or HCO_3^- generation rate will depend on the CO_2 and HCO_3^- concentrations and pH in the coral tissue, and the rates and net direction of the reaction will likely vary in different regions of the coral. Nonetheless, the gross generation rates put limits on the net generation rates.

Assuming the CO_2 concentration in the coral is 10 µmol l^{-1}, similar to seawater concentrations, the gross iCA-catalyzed HCO_3^- generation rate for *O. faveolata* would be 3.4×10^{-4} mol cm^{-2} h^{-1}. This rate is many orders of magnitude higher than the net photosynthetic rate we measured for *O. faveolata* (5×10^{-7} mol cm^{-2} h^{-1}), and as calcification rates are generally comparable to or less than the net photosynthetic rate, the gross HCO_3^- generation rate also greatly exceeds the calcification rate. Similarly, the gross HCO_3^- generation

The Journal of Experimental Biology (2015) 218, 2039-2048 doi:10.1242/jeb.118182

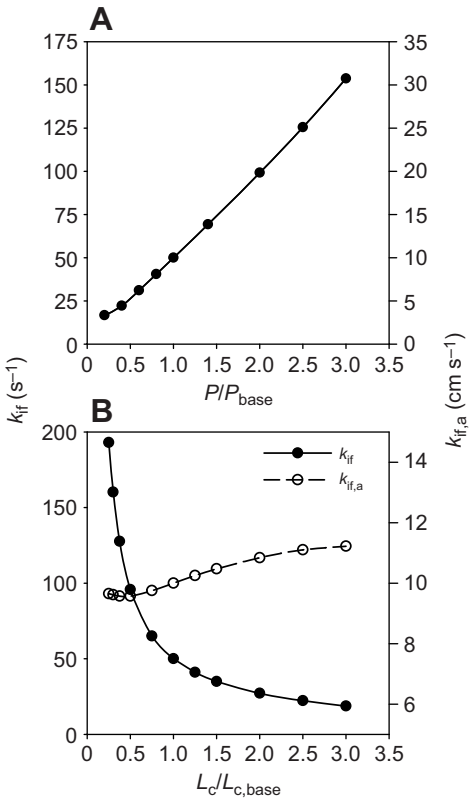

Fig. 7. Effect of photosynthetic rate and tissue thickness on iCA activity required to maintain constant CO_2 deviations from equilibrium in the spatially resolved model of coral C_i processing. iCA activity is given normalized to coral tissue volume (k_{if}) and to coral surface area ($k_{if,a}$). (A) Photosynthetic rate, P; (B) tissue thickness, L_c. On the x-axes, the parameters are plotted relative to baseline values for photosynthetic rate (P_{base}=1×10^{-6} mol cm^{-2} h^{-1}) and tissue thickness ($L_{c,base}$=2 mm).

rates for *P. astreoides* and *S. radians* greatly exceed net photosynthetic rates. Thus, there is in principle sufficient iCA activity to convert CO_2 imported for photosynthesis to HCO_3^- (Fig. 1, arrow 2), and to convert respired CO_2 to HCO_3^- for calcification (Fig. 1, arrows 4 and 5). The gross CO_2 generation rate, calculated assuming that the average internal pH is 7.4 (Venn et al., 2009, 2011) and that the internal HCO_3^- concentration is 1.8 mmol l^{-1}, similar to seawater, is 1.6×10^{-3} mol cm^{-2} h^{-1}. Again, the gross CO_2 production rate is orders of magnitude higher than the net photosynthetic rate, showing there is sufficient iCA activity to produce CO_2 for uptake by symbiotic algae (Fig. 1, arrow 3). These gross production rates are of course maximal net production rates, and use estimates for internal CO_2, HCO_3^- and H^+ concentrations. But the fact that they are many orders of magnitude higher than the required net production rates suggests that there should be enough iCA capacity to fulfill any of these roles.

For a more detailed assessment, a spatially resolved model of C_i processing in the coral tissue was developed. Because C_i processing pathways have not been fully defined in corals, the model is necessarily schematic, and iCAs are used in as many roles as possible to maximize the need for iCA activity. The model was first run with an iCA activity similar to that measured in *O. faveolata* and *P. astreoides* (50 s^{-1}) distributed homogeneously throughout the coral tissue. This iCA activity and distribution are sufficient to support realistic rates of photosynthesis and calcification in the model, though they are only just sufficient to support a realistic calcification rate (Fig. 6). The ability of the measured iCA activity to catalyze the multiple hydrations and dehydrations needed to move C_i from seawater to *Symbiodinium* and to the calcifying fluid is consistent with the simpler calculations showing that the potential CO_2 and HCO_3^- generation rates from iCA greatly exceed those required for individual steps in the C_i processing pathways. The measured iCA activity is neither deficient nor greatly excessive as shown by model runs with 10-fold higher or lower iCA activity. Higher iCA activity (500 s^{-1}) does not offer any direct benefit in the model, and the lower iCA activity (5 s^{-1}) is only barely sufficient to meet the C_i requirements of photosynthesis and does not supply enough C_i to support measured rates of calcification.

The fact that a homogeneous distribution of iCA is capable of meeting C_i needs does not imply that iCA is or should be homogeneously distributed. The calcifying fluid and oral endoderm would benefit from greater CA activity as shown by the significant deviation of CO_2 from equilibrium with HCO_3^- in these model layers (Fig. 6). The observed localization of CA in the calicoblastic cells and potentially in the calcifying fluid (Isa and Yamazato, 1984; Tambutte et al., 2007; Moya et al., 2008) may be particularly helpful as $CaCO_3$ is being rapidly precipitated from a very thin layer of calcifying fluid (~3 µm thick; Venn et al., 2011), necessitating high rates of CO_2 conversion to HCO_3^- within a very small volume of fluid. It may also be detrimental to have CA activity in all parts of the tissue. For example, cyanobacteria lack CA in the cytoplasm, allowing them to accumulate HCO_3^-, and if CA is artificially expressed in the cytoplasm, HCO_3^- is rapidly converted to CO_2, which leaks out of the cell (Price and Badger, 1989). Storage of HCO_3^- in a tissue layer or vacuole within the coral may require CA to be absent from that space.

Differences among species

Coral iCA activities were determined in three species of coral, *O. faveolata* and *P. astreoides*, which inhabit offshore reefs, *S. radians*, which is found in the shallow, soft-bottomed environment of Florida Bay. When normalized by tissue volume, the two reef species show similar iCA activity, while *S. radians* has about 10-fold higher iCA activity (Fig. 3). The slow circulation in the bay may limit the transfer of C_i between bulk seawater and the surface of *S. radians*, requiring increased iCA activity to help facilitate C_i acquisition. Lesser et al. (1994) showed that total CA activity of the coral *Pocillopora damicornis* increased when exposed to low flow in a controlled flume experiment. However, *S. radians* also has the thinnest effective tissue thickness (tissue volume per unit surface area; Table 1) of the corals surveyed and when coral iCA activity is instead normalized by surface area we find that *S. radians* and *O. faveolata* have similar iCA activities with *P. astreoides* having ~50% lower iCA activity (Fig. 3).

As coral iCA is involved in C_i supply for photosynthesis and calcification, the similar rates of photosynthesis (and so presumably of calcification) per unit surface area for these corals would suggest that they need similar amounts of iCA on an areal basis, an intuition that we explored with the spatially resolved model of C_i processing. When photosynthetic rates were varied, the iCA activity required to maintain constant effectiveness of the C_i processing system in the model, as indicated by CO_2 deviations from equilibrium, increased or decreased approximately linearly with the photosynthetic rate (Fig. 7A). Next, photosynthetic rates were kept constant, while coral tissue thickness was varied. The iCA activity per unit surface area required to maintain constant CO_2 deviations from equilibrium remained essentially constant, though there was a slight increase in iCA activity per unit surface area as tissue thickness increased, a result of its role in facilitated diffusion of C_i through the tissue layers (Fig. 7B; Enns, 1967). In contrast, the iCA activity per unit volume must increase dramatically as the metabolic rates are squeezed into a thinner tissue layer and can decrease as the tissue expands. This

analysis suggests that the primary reason iCA activity per unit volume is higher in *S. radians* is because of the thinner effective tissue thickness in this organism and not because of environmental differences, whereas the iCA activity per unit surface area is more similar among species because the metabolic processes iCAs are involved in are relatively constant on an areal basis.

In summary, we have developed a method to measure the absolute iCA activities of corals and have applied this method to three species of scleractinian corals found in the Florida Keys. A key advantage of these absolute measurements is that they allow us to assess the ability of measured iCA activity to fulfill proposed roles in photosynthesis and calcification. Using simple back of the envelope calculations and a more detailed spatially resolved model, we showed that the iCA activities are capable of sustaining the rapid rates of CO_2/HCO_3^- interconversion required to deliver C_i for photosynthesis and calcification.

MATERIALS AND METHODS

Coral collection and maintenance

Fragments of *Orbicella* (previously *Montastraea*) *faveolata*, *Porites astreoides* and *Siderastrea radians* were collected from Little Grecian reef and Florida Bay in Key Largo, FL, USA, in August of 2013 as permitted by the Florida Keys National Marine Sanctuary (FKNMS-2011-093, FKNMS-2014-015). Exposed skeleton was covered with modeling clay, and the colonies were maintained in closed circulation tanks filled with reef seawater, allowing at least 2 days of recovery after collection prior to experimentation. The tank was exposed to a natural light regime, with shading added at midday to keep solar irradiance below 600 µmol photons m^{-2} s^{-1}. Coral surface area was measured using an aluminium foil method (Marsh, 1970). Coral tissue thickness was measured on freshly fragmented corals with an ocular micrometer on a stereomicroscope (Leica WILD M3Z, Wetzlar, Germany). The thickness varied between polyps and the coenosarc and multiple measurements across the colony were averaged to obtain an average tissue thickness (L_c) for each species (Table 1). The tissue of *P. astreoides* and *S. radians* is intermingled with the skeleton and the fractional occupancy of tissue (ϕ, porosity of the skeleton) was estimated from cross-sectional images of the fragmented coral colonies. The images were analyzed with ImageJ using color and brightness characteristics to segment the image between tissue and skeletal fractions. The effective tissue thickness, the thickness of the tissue if it was not intermingled with skeleton, was calculated as ϕL_c. Algal symbiont clades as determined by denaturing gradient gel electrophoresis (DGGE) analysis of the ITS2 sequence were: *O. faveolata* – B1; *P. astreoides* – A4a; *S. radians* – B5 (LaJeunesse et al., 2003).

Coral eCA activity

eCA activity was measured on intact coral fragments using an ^{18}O-removal technique described in Tansik et al. (in press). Briefly, a water-jacketed chamber is interfaced to a membrane inlet mass spectrometer (MIMS; QMS 220M2, Pfeiffer Vacuum, Asslar, Germany) that allows continuous monitoring of CO_2 isotopes. The chamber is filled with C_i-free artificial seawater (ASW), buffered with 20 mmol l^{-1} Tris at pH 8.0, and ^{13}C-^{18}O-labeled C_i is added to the chamber. After monitoring ^{18}O-removal for approximately 15 min to determine the background rate of removal, a coral fragment is added to the chamber and ^{18}O-removal catalyzed by the coral is monitored for a further 10 min. Finally 100 µmol l^{-1} of the eCA inhibitor dextran-bound AZ is added to the chamber and ^{18}O-removal is monitored for 10 min. The data are fitted to a model of ^{18}O-removal that accounts for background removal rates, iCA activity and eCA activity, with the measurement of interest being eCA activity.

iCA activity and mass transfer coefficients of symbiotic algae

To measure the iCA activity and mass transfer coefficients of the symbiotic algae, the algae were first isolated from the coral. Coral tissue was removed from the skeleton with an airbrush (Paasche, Chicago, IL, USA) using ASW with 20 mmol l^{-1} Tris at pH 8.0 and containing a protease inhibitor cocktail (complete protease inhibitor cocktail mini tablets, 1 tablet per 20 ml). The algae were then separated from the coral homogenate by centrifugation at 2350 ***g*** for 5 min. iCA activity and the CO_2 and HCO_3^- mass transfer coefficients were measured on the algae using an ^{18}O-removal method described previously (Tu et al., 1978; Hopkinson et al., 2011). Absolute iCA activity was inferred by fitting a model that treats the interior of the cell as a single homogeneous compartment to the ^{18}O-removal data. The mass transfer coefficients describe controls on the flux of CO_2 and HCO_3^- into the cells, which is primarily controlled by the diffusive boundary layer and cell membrane permeability.

CA activity of the coral tissue homogenate

The CA activity of the coral tissue homogenate from which symbiotic algae had been removed ('purified coral tissue homogenate') was measured using an ^{18}O-removal technique. ^{13}C-^{18}O-labeled C_i (2 mmol l^{-1}) was added to assay buffer (C_i-free ASW, 20 mmol l^{-1} Tris at pH 8.0) in a small MIMS chamber that holds ~1 ml of solution. Temperature in the chamber was maintained at 28°C with a water jacket. ^{18}O-CO_2 species were monitored with the MIMS system for approximately 10 min to determine the background rate of removal due to CO_2 hydration/HCO_3^- dehydration. Then a sample of the purified homogenate was added to the chamber and the accelerated ^{18}O-removal rate was monitored for approximately 10 min. In some cases a CA inhibitor, 10 µmol l^{-1} AZ, was then added to confirm that the accelerated ^{18}O-removal rate was due to CA activity. A sample of the purified homogenate was preserved in formalin to determine the residual concentration of symbiotic algae in the sample via microscopy.

^{18}O-removal model for coral iCA determination

The ^{18}O-removal data obtained from the coral homogenate were analyzed using a model that accounts for the effects of background CO_2 hydration/HCO_3^- dehydration, coral eCA activity and residual algal iCA activity on ^{18}O-removal, attributing the remaining ^{18}O-removal to coral iCA. The model treats coral eCA and coral iCA as being homogeneously distributed throughout the assay solution, while the algae are treated as a separate compartment with fluxes between the compartments parameterized using mass transfer coefficients. The model is described by the following system of differential equations:

$$\frac{d\mathbf{c}_e}{dt} = -(k_{uf} + k_{sf,d} + k_{if,d})\mathbf{c}_e + (k_{ur} + k_{sr,d} + k_{ir,d})\mathbf{H}\mathbf{b}_e + f_c N(\mathbf{c}_i - \mathbf{c}_e), \quad (3)$$

$$\frac{d\mathbf{b}_e}{dt} = (k_{uf} + k_{sf,d} + k_{if,d})\mathbf{G}\mathbf{c}_e - (k_{ur} + k_{sr,d} + k_{ir,d})\mathbf{b}_e + f_b N(\mathbf{b}_i - \mathbf{b}_e), \quad (4)$$

$$\frac{d\mathbf{c}_i}{dt} = -k_{cf}\mathbf{c}_i + k_{cr}\mathbf{H}\mathbf{b}_i + \frac{f_c}{V_{cell}}(\mathbf{c}_e - \mathbf{c}_i), \quad (5)$$

$$\frac{d\mathbf{b}_i}{dt} = k_{cf}\mathbf{G}\mathbf{c}_i - k_{cr}\mathbf{b}_i + \frac{f_b}{V_{cell}}(\mathbf{b}_e - \mathbf{b}_i). \quad (6)$$

The notation is detailed in Table 1. For simplicity, rate constants for coral eCA- and iCA-catalyzed hydration and dehydration are given as the first-order rates constants when diluted in the assay ($k_{sf,d}$, diluted eCA-catalyzed hydration rate; $k_{if,d}$, diluted iCA-catalyzed hydration rate). These are related to the intrinsic rate constants in the intact coral by the following equations that correct for dilution in the assay:

$$k_{sf} = k_{sf,d}\left(\frac{V_{hom}V_e}{A_c V_{add}}\right), \quad (7)$$

$$k_{if} = k_{if,d}\left(\frac{V_{hom}V_e}{A_c L_c \phi V_{add}}\right). \quad (8)$$

The coral iCA can alternatively be normalized to coral surface area rather than volume:

$$k_{if,a} = k_{if,d}\left(\frac{V_{hom}V_e}{A_c V_{add}}\right). \quad (9)$$

The only unknown parameters in these equations are the coral iCA-catalyzed CO_2 hydration and HCO_3^- dehydration rate constants, which are related to each other by the CO_2/HCO_3^- equilibrium constant, assuming microscopic reversibility. Consequently, there is effectively only one unknown, k_{if}, the first-order rate constant for the coral iCA-catalyzed CO_2 hydration, which was determined by optimizing the model fit to the ^{18}O-CO_2 data. The background rate constants for CO_2 hydration/dehydration (k_{uf}, k_{ur}) were determined from the ^{18}O-removal rate prior to the addition of homogenate. The coral eCA activity (k_{sf}, k_{sr}) was measured as described above, as was the algal iCA activity (k_{cf}, k_{cr}) and the CO_2 and HCO_3^- mass transfer coefficients (f_c, f_b). The volume of the algal cells was determined from measurements of cell radius, approximating the cells as spheres.

Spatially resolved model of coral C_i processing

A one-dimensional model of C_i processing in coral tissues was developed to assess the potential functions of iCAs and the iCA activity required to perform these roles. The model considers CO_2 and HCO_3^- in the diffusive boundary layer adjacent to the coral surface, the oral ectoderm, the oral endoderm, the coelenteron, a combined aboral ectoderm and endoderm, and the calcifying fluid (supplementary material Fig. S1). CO_3^{2-} is treated implicitly as part of the HCO_3^- pool as equilibrium between these two species is rapidly established (Zeebe and Wolf-Gladrow, 2001). CO_2 and HCO_3^- are transported by diffusion within the model compartments, and CO_2 diffuses passively through membrane barriers separating compartments, while HCO_3^- only traverses membranes via active membrane-embedded transporters. Photosynthesis occurs in the oral endoderm; respiration occurs in all the tissue layers and is distributed between the compartments based on the thickness of each tissue layer; calcification occurs in the calcifying fluid. In each layer of the model the following generic equations are solved:

$$\frac{d[CO_2]}{dt} = -k_f[CO_2] + k_r[HCO_3^-] + \frac{D_c}{z}\left(\frac{d[CO_2]}{dz}\right) + T + M, \quad (10)$$

$$\frac{d[HCO_3^-]}{dt} = k_f[CO_2] - k_r[HCO_3^-] + \frac{D_b}{z}\left(\frac{d[HCO_3^-]}{dz}\right) + T + M. \quad (11)$$

The first two terms describe the chemical reactions: hydration of CO_2 and dehydration of HCO_3^-, while the third term describes diffusion, and the final two terms represent transport (T) and the metabolic reactions (M): photosynthesis, respiration and calcification. k_f and k_r are the first-order rate constants for CO_2 hydration and HCO_3^- dehydration. D_c and D_b are the diffusion coefficients for CO_2 and HCO_3^-, respectively, and z is the thickness of the model layer. pH in each tissue layer was set as shown in supplementary material Fig. S1, based on literature values (Venn et al., 2009, 2011; Ries, 2011) except that the pH in the oral tissue layers had to be elevated somewhat to achieve a net CO_2 influx. HCO_3^- transport rates between the tissue layers were set to obtain steady-state concentrations in each layer, delivering C_i as needed for photosynthesis and calcification, and removing respired CO_2 (supplementary material Fig. S1).

Rates of gross photosynthesis (1×10^{-6} mol cm^{-2} h^{-1}), respiration (5×10^{-7} mol cm^{-2} h^{-1}) and calcification (1.7×10^{-7} mol cm^{-2} h^{-1}) measured for *O. faveolata* were used as base rates in the model. The model was designed to maximize the need for iCA, employing iCA in as many consistent roles as possible as shown in supplementary material Fig. S1: conversion of imported and respired CO_2 to HCO_3^- in the oral ectoderm, conversion of HCO_3^- to CO_2 for uptake by *Symbiodinium* in the oral endoderm, and conversion of respired CO_2 to HCO_3^- in the aboral tissue and calcifying fluid. CO_2 and HCO_3^- concentrations were set at typical seawater values at the outer edge of the diffusive boundary layer and the model was then run until a steady state was reached.

Acknowledgements

We thank Dustin Kemp and Clinton Oakley for assistance with coral collection and maintenance, and Virginia Weis for advice on measurement of carbonic anhydrase activity in corals. Permission to collect corals was granted by the Florida Keys National Marine Sanctuary.

Competing interests

The authors declare no competing or financial interests.

Author contributions

B.M.H., A.L.T. and W.K.F. designed the project. A.L.T. conducted the experiments. B.M.H. developed and executed the models. B.M.H., A.L.T. and W.K.F. wrote the paper.

Funding

This work was supported by a National Science Foundation grant to B.M.H. and W.K.F. [EF1315944] and a Sloan Foundation Fellowship to B.M.H.

Supplementary material

Supplementary material available online at
http://jeb.biologists.org/lookup/suppl/doi:10.1242/jeb.118182/-/DC1

References

Al-Moghrabi, S., Goiran, C., Allemand, D., Speziale, N. and Jaubert, J. (1996). Inorganic carbon uptake for photosynthesis by the symbiotic coral-dinoflagellate association II. Mechanisms for bicarbonate uptake. *J. Exp. Mar. Biol. Ecol.* **199**, 227-248.

Badger, M. R. (2003). The roles of carbonic anhydrases in photosynthetic CO_2 concentrating mechanisms. *Photosynth. Res.* **77**, 83-94.

Bertucci, A., Tambutte, E., Tambutte, S., Allemand, D. and Zoccola, D. (2010). Symbiosis-dependent gene expression in coral-dinoflagellate association: cloning and characterization of a P-type H^+-ATPase gene. *Proc. R. Soc. B Biol. Sci.* **277**, 87-95.

Bertucci, A., Tambutté, S., Supuran, C. T., Allemand, D. and Zoccola, D. (2011). A new coral carbonic anhydrase in *Stylophora pistillata*. *Mar. Biotechnol.* **13**, 992-1002.

Bertucci, A., Moya, A., Tambutté, S., Allemand, D., Supuran, C. T. and Zoccola, D. (2013). Carbonic anhydrases in anthozoan corals-A review. *Bioorg. Med. Chem.* **21**, 1437-1450.

Boron, W. F. (2004). Regulation of intracellular pH. *Adv. Physiol. Educ.* **28**, 160-179.

Burton, E. A. and Walter, L. M. (1987). Relative precipitation rates of aragonite and Mg calcite from seawater: temperature or carbonate ion control. *Geology* **15**, 111-114.

Clode, P. L. and Marshall, A. T. (2002). Low temperature FESEM of the calcifying interface of a scleractinian coral. *Tissue Cell* **34**, 187-198.

Cohen, A. L. and McConnaughey, T. A. (2003). Geochemical perspectives on coral mineralization. In *Biomineralization*, Vol. 54 (ed. P. M. Dove, J. J. DeYoreo and S. Weiner), pp. 151-187. Chantilly: Mineralogical Society of America.

Enns, T. (1967). Facilitation by carbonic anhydrase of carbon dioxide transport. *Science* **155**, 44-47.

Freeman, J. A. and Wilbur, K. M. (1948). Carbonic anhydrase in molluscs. *Biol. Bull.* **94**, 55-59.

Furla, P., Allemand, D. and Orsenigo, M. N. (2000a). Involvement of H^+-ATPase and carbonic anhydrase in inorganic carbon uptake for endosymbiont photosynthesis. *Am. J. Physiol. Regul. Integr. Comp. Physiol.* **278**, R870-R881.

Furla, P., Galgani, I., Durand, I. and Allemand, D. (2000b). Sources and mechanisms of inorganic carbon transport for coral calcification and photosynthesis. *J. Exp. Biol.* **203**, 3445-3457.

Gagnon, A. C., Adkins, J. F. and Erez, J. (2012). Seawater transport during coral biomineralization. *Earth Planet. Sci. Lett.* **329-330**, 150-161.

Goreau, T. F. (1959). The physiology of skeleton formation in corals. I. A method for measuring the rate of calcium deposition by corals under different conditions. *Biol. Bull.* **116**, 59-75.

Grasso, L. C., Maindonald, J., Rudd, S., Hayward, D. C., Saint, R., Miller, D. J. and Ball, E. E. (2008). Microarray analysis identifies candidate genes for key roles in coral development. *BMC Genomics* **9**, 540.

Gutknecht, J., Bisson, M. A. and Tosteson, F. C. (1977). Diffusion of carbon dioxide through lipid bilayer membranes: effects of carbonic anhydrase, bicarbonate, and unstirred layers. *J. Gen. Physiol.* **69**, 779-794.

Henry, R. P. (1996). Multiple roles of carbonic anhydrase in cellular transport and metabolism. *Ann. Rev. Physiol.* **58**, 523-538.

Hohn, S. and Merico, A. (2012). Modelling coral polyp calcification in relation to ocean acidification. *Biogeosciences* **9**, 4441-4454.

Hopkinson, B. M., Dupont, C. L., Allen, A. E. and Morel, F. M. M. (2011). Efficiency of the CO_2-concentrating mechanism of diatoms. *Proc. Natl. Acad. Sci. USA* **108**, 3830-3837.

Hopkinson, B. M., Meile, C. and Shen, C. (2013). Quantification of extracellular carbonic anhydrase activity in two marine diatoms and investigation of its role. *Plant Physiol.* **162**, 1142-1152.

Isa, Y. and Yamazato, K. (1984). The distribution of carbonic anhydrase in a staghorn coral, *Acropora hebes* (Dana). *Galaxea* **3**, 25-36.

Kenkel, C. D., Meyer, E. and Matz, M. V. (2013). Gene expression under chronic heat stress in populations of the mustard hill coral (*Porites astreoides*) from different thermal environments. *Mol. Ecol.* **22**, 4322-4334.

Kikutani, S., Tanaka, R., Yamazaki, Y., Hara, S., Hisabori, T., Kroth, P. G. and Matsuda, Y. (2012). Redox regulation of carbonic anhydrases via thioredoxin in chloroplast of the marine diatom *Phaeodactylum tricornutum*. *J. Biol. Chem.* **287**, 20689-20700.

LaJeunesse, T. C., Loh, W. K. W., van Woesik, R., Hoegh-Guldberg, O., Schmidt, G. W. and Fitt, W. K. (2003). Low symbiont diversity in southern Great Barrier Reef corals relative to those of the Caribbean. *Limnol. Oceanogr.* **48**, 2046-2054.

Leggat, W., Badger, M. R. and Yellowlees, D. (1999). Evidence for an inorganic carbon-concentrating mechanism in the symbiotic dinoflagellate *Symbiodinium* sp. *Plant Physiol.* **121**, 1247-1255.

Lesser, M. P., Weis, V. M., Patterson, M. R. and Jokiel, P. L. (1994). Effects of morphology and water motion on carbon delivery and productivity in the reef coral, *Pocillopora damincornis* (Linnaeus): diffusion barriers, inorganic carbon limitation, and biochemical plasticity. *J. Exp. Mar. Biol. Ecol.* **178**, 153-179.

Marsh, J. A. (1970). Primary productivity of reef-building calcareous red algae. *Ecology* **51**, 255-263.

Moya, A., Tambutte, S., Bertucci, A., Tambutte, E., Lotto, S., Vullo, D., Supuran, C. T., Allemand, D. and Zoccola, D. (2008). Carbonic anhydrase in the scleractinian coral *Stylophora pistillata*: characterization, localization, and role in biomineralization. *J. Biol. Chem.* **283**, 25475-25484.

Moya, A., Huisman, L., Ball, E. E., Hayward, D. C., Grasso, L. C., Chua, C. M., Woo, H. N., Gattuso, J.-P., Forêt, S. and Miller, D. J. (2012). Whole transcriptome analysis of the coral *Acropora millepora* reveals complex responses to CO_2-driven acidification during the initiation of calcification. *Mol. Ecol.* **21**, 2440-2454.

Nakamura, T., Nadaoka, K. and Watanabe, A. (2013). A coral polyp model of photosynthesis, respiration and calcification incorporating a transcellular ion transport mechanism. *Coral Reefs* **32**, 779-794.

Price, G. D. and Badger, M. R. (1989). Expression of human carbonic anhydrase in the cyanobacterium *Synechococcus* PCC7942 Creates a high CO_2-requiring phenotype: evidence for a central role for carboxysomes in the CO_2 concentrating mechanism. *Plant Physiol.* **91**, 505-513.

Ries, J. B. (2011). A physicochemical framework for interpreting the biological calcification response to CO_2-induced ocean acidification. *Geochim. Cosmochim. Acta* **75**, 4053-4064.

Silverman, D. N. (1982). Carbonic anhydrase: oxygen-18 exchange catalyzed by an enzyme with rate-contributing proton-transfer steps. *Methods Enzymol.* **87**, 732-752.

Tambutte, S., Tambutte, E., Zoccola, D., Caminiti, N., Lotto, S., Moya, A., Allemand, D. and Adkins, J. (2007). Characterization and role of carbonic anhydrase in the calcification process of the azooxanthellate coral *Tubastrea aurea*. *Mar. Biol.* **151**, 71-83.

Tambutte, S., Holcomb, M., Ferrier-Pages, C., Reynaud, S., Tambutte, E., Zoccola, D. and Allemand, D. (2011). Coral biomineralization: from the gene to the environment. *J. Exp. Mar. Biol. Ecol.* **408**, 58-78.

Tansik, A. L., Fitt, W. K. and Hopkinson, B. M. (2015). External carbonic anhydrase activity in three Caribbean corals: quantification of activity and role in CO_2 uptake. *Coral Reefs.* doi:10.1007/s00338-015-1289-8

Tu, C., Wynns, G. C., McMurray, R. E. and Silverman, D. N. (1978). CO_2 kinetics in red cell suspensions measured by ^{18}O exchange. *J. Biol. Chem.* **253**, 8178-8184.

Tu, C. K., Acevedo-Duncan, M., Wynns, G. C. and Silverman, D. N. (1986). Oxygen-18 exchange as a measure of accessibility of CO_2 and HCO_3^- to carbonic anhydrase in *Chlorella vulgaris* (UTEX 263). *Plant Physiol.* **80**, 997-1001.

Venn, A. A., Tambutte, E., Lotto, S., Zoccola, D., Allemand, D. and Tambutte, S. (2009). Imaging intracellular pH in a reef coral and symbiotic anemone. *Proc. Natl. Acad. Sci. USA* **106**, 16574-16579.

Venn, A., Tambutté, E., Holcomb, M., Allemand, D. and Tambutté, S. (2011). Live tissue imaging shows reef corals elevate pH under their calcifying tissue relative to seawater. *PLoS ONE* **6**, e20013.

Weis, V. M. (1993). Effect of dissolved inorganic carbon concentration on the photosynthesis of the symbiotic sea anemone *Aiptasia pulchella* Carlgren: role of carbonic anhydrase. *J. Exp. Mar. Biol. Ecol.* **174**, 209-225.

Weis, V. M., Smith, G. J. and Muscatine, L. (1989). A CO_2 supply mechanism in zooxanthellate cnidarians: role of carbonic anhydrase. *Mar. Biol.* **100**, 195-202.

Wilbur, K. M. and Jodrey, L. H. (1955). Studies on shell formation. V. the inhibition of shell formation by carbonic anhydrase inhibitors. *Biol. Bull.* **108**, 359-365.

Zeebe, R. E. and Wolf-Gladrow, D. (2001). *CO_2 in Seawater: Equilibrium, Kinetics, Isotopes*. Amsterdam: Elsevier.

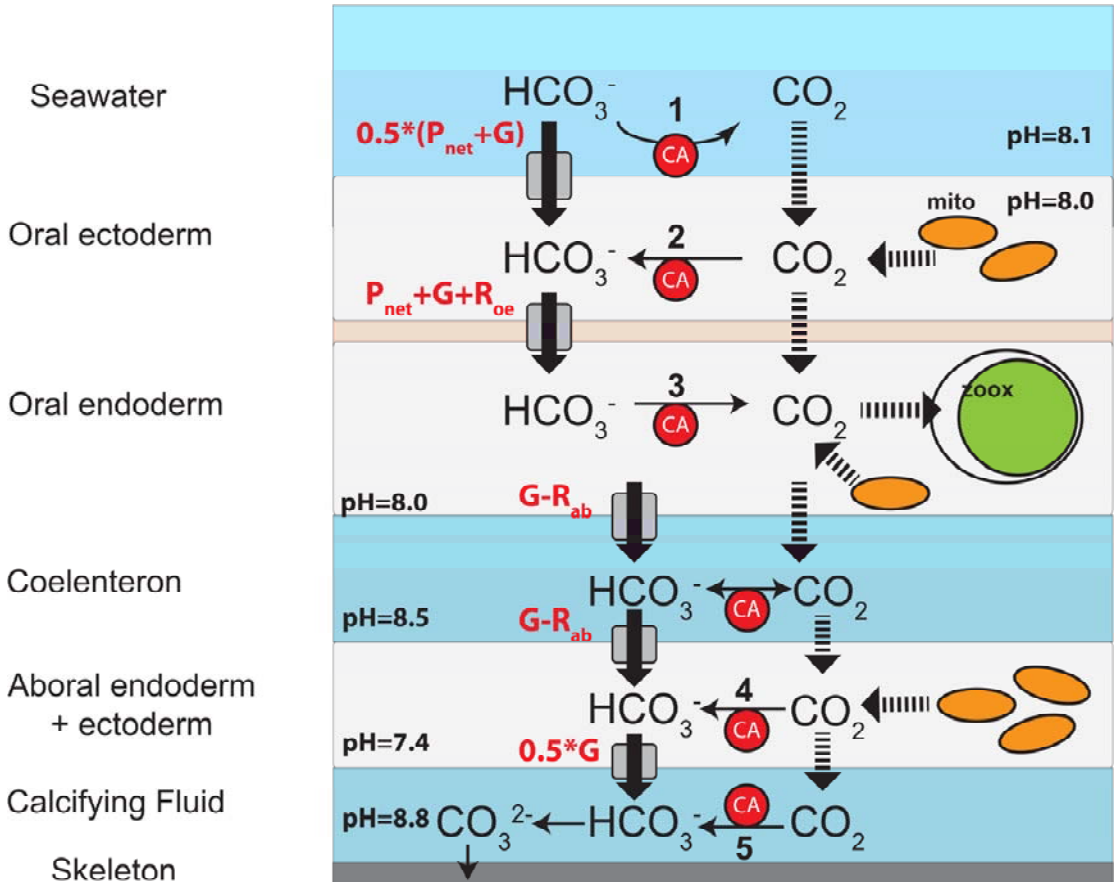

Fig. S1. Layers and fluxes in the spatially resolved model of coral C_i processing. The model considers active HCO_3^- fluxes (solid arrows, with specified rates in red text beside each arrow) and diffusive CO_2 fluxes (dashed arrows) between tissue compartments, and the production of CO_2 by mitochondrial respiration (orange ovals), consumption of CO_2 by *Symbiodinium* (green circle), and loss of CO_3^{2-} through $CaCO_3$ precipitation in the calcifying fluid. CO_2 and HCO_3^- inter-conversion in each layer is catalyzed by carbonic anhydrase (red circles) and the CO_2/HCO_3^- equilibrium is affected by pH as indicated in each layer.